

# Gravitational and Magnetic Instabilities in Disks

By TOMOYUKI HANAWA

Department of Astrophysics, School of Science, Nagoya University, Chikusa-ku, Nagoya  
464-01, Japan

We study the instabilities of the galactic disk induced by magnetic fields and self-gravity of the disk. Based on numerical computations, we discuss the linear and non-linear evolution of the instabilities. Gravity, rotation, gas pressure and magnetic force commonly have the timescale of  $10^8$  yr in the galactic disk. Accordingly, all these forces participate in the instabilities of the galactic gaseous disk. Our numerical computations take account of the rotation and magnetic shear, and also of self-gravity and non-uniform magnetic fields. It is shown that the stability of the present gas disk is very different from that of a gas-rich (presumably young) disk.

## 1. Introduction

The galactic disk is inhomogeneous to a high degree. Up to the present, 90% of the disk matter has been converted into stars. The rest of the disk consists of molecular clouds, HI clouds and coronal gas, the densities and temperatures of which range from  $10^{-2}$  cm $^{-3}$  to  $10^5$  cm $^{-3}$  and from 10 to  $10^6$  K, respectively. The inhomogeneity of the gas disk will be attributed in part to instability of a homogeneous disk. Magnetic fields and self-gravity of the gas induce the Parker and the Jeans instabilities. In this paper we discuss these instabilities, taking account of the rotation and gravity of stars. In Section 2 we give an overview of the dynamical processes in the galactic disk and their timescales. In Section 3 we review the linear stability of the galactic disk according to Hanawa *et al.* (1992, hereafter HNN). In Section 4 the non-linear evolution of the instability is discussed based on numerical simulations. A brief summary is given in Section 5.

## 2. Timescale

First we review the dynamical processes forming dense clouds in the galactic disk. Figure 1 summarises main factors and processes involved. Gravity acts for the formation of dense clouds through the Jeans and Parker instabilities. Dense cloud-formation is suppressed by the pressure of thermal motion and centrifugal force due to rotation. Although the magnetic field suppresses the contraction of clouds by its pressure, it forms clouds through the Parker instability and extracts angular momentum from the cloud's contraction. The thick and thin arrows denote the processes initiating and suppressing dense cloud-formation, respectively. The dashed arrow denotes the different process.

These various processes have almost the same timescale of  $10^8$  yr in the galactic disk (see the comment by Shore in the Discussion). The galactic rotation has the frequency

$$\Omega = 8.40 \times 10^{-15} \left( \frac{v_\phi}{220 \text{ km s}^{-1}} \right) \left( \frac{r}{8.5 \text{ kpc}} \right)^{-1} \text{ Hz} . \quad (2.1)$$

The timescale for gravitational collapse is evaluated to be

$$\nu_J = \sqrt{4\pi G\rho} = 1.18 \times 10^{-15} \left( \frac{n}{1 \text{ cm}^{-3}} \right)^{-1/2} \text{ Hz} , \quad (2.2)$$

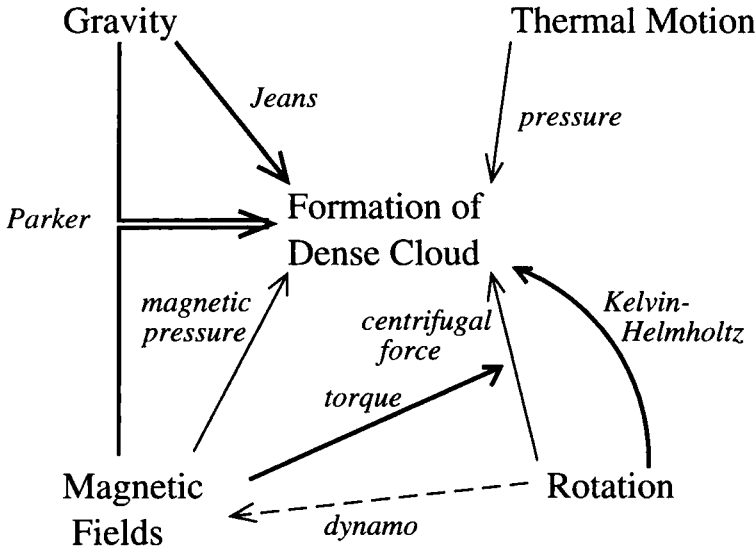


FIGURE 1. Dynamical processes working in the galactic disk. The thick and thin arrows denote those initiating and suppressing the formation of dense clouds, respectively. The dashed arrow denotes otherwise.

for the homogeneous medium having the mass density,  $\rho$ , and the equivalent nucleon number density,  $n$ . The magnetic force propagates with the frequency,

$$\nu_m = 1.34 \times 10^{-15} \left( \frac{B}{3 \mu\text{G}} \right) \left( \frac{n}{1 \text{ cm}^{-3}} \right)^{-1/2} \left( \frac{\lambda}{1 \text{ kpc}} \right)^{-1} \text{ Hz}, \quad (2.3)$$

where  $B$  and  $\lambda$  are the magnetic flux density and the wavelength, respectively. Similarly the sound wave has the frequency

$$\nu_s = 1.43 \times 10^{-15} \left( \frac{c_s}{7 \text{ km s}^{-1}} \right) \left( \frac{\lambda}{1 \text{ kpc}} \right)^{-1} \text{ Hz}, \quad (2.4)$$

where  $c_s$  denotes the sound speed. The timescale of  $10^8$  yr corresponds to the frequency of  $1.77 \times 10^{-15}$  Hz. Thus the gas dynamics is controlled by many equally dominant factors in the galactic disk.

### 3. Linear stability

Recently HNN analysed the stability of the galactic gaseous disk, taking account of the self-gravity of the gas and stars as well as rotation and magnetic fields. We approximated the equilibrium galactic disk by a uniformly rotating gaseous sheet in which the density and magnetic field are uniform in the horizontal ( $x$ - and  $y$ -) directions. The vertical ( $z$ -) component of the gravity in equilibrium was taken to be

$$g_{z,0} = \left\{ 6.8 \tanh \left[ 3.2 \left( \frac{z}{1 \text{ kpc}} \right) \right] + 1.7 \left( \frac{z}{1 \text{ kpc}} \right) \right\} \times 10^{-9} \text{ cm s}^{-2}, \quad (3.5)$$

in order to reproduce the observed value in the solar neighbourhood (Oort 1965). The ratio of the gas pressure to the magnetic pressure ( $\beta$ ) was for simplicity assumed to be constant. The gas was assumed to be isothermal in the region of  $z \leq z_d$  and the sound speed ( $c_s$ ) was taken to be constant there. The HNN equilibrium model is specified by

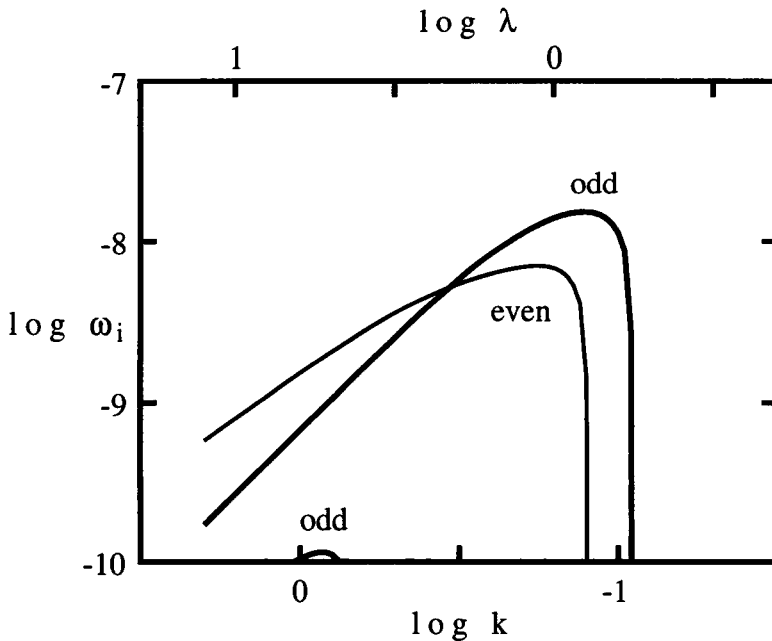


FIGURE 2. The stability diagram for perturbations with a wave number parallel to the magnetic field,  $k$ . The ordinate and abscissa are the wave number in units of  $\text{kpc}^{-1}$  and the growth rate ( $\omega_i$ ) in units of  $\text{yr}^{-1}$ . The thick and thin curves denote the dispersion relations for odd and even modes against the galactic plane, respectively. The equilibrium model parameters are set  $n_c = 1 \text{ cm}^{-3}$ ,  $B_c = 3.23 \mu\text{G}$ ,  $v_\varphi = 220 \text{ km s}^{-1}$ ,  $c_s = 5 \text{ km s}^{-1}$ , and  $z_d = 200 \text{ pc}$ . Reproduced from Figure 1a of HNN.

five model parameters, the density on the galactic plane ( $n_c$ ), the magnetic flux density on the plane ( $B_c$ ), the rotation velocity, ( $v_\varphi$ ), the sound speed ( $c_s$ ), and  $z_d$ .

Figure 2 shows the dispersion relation of HNN Model 1 of which parameters are set  $n_c = 1 \text{ cm}^{-3}$ ,  $B_c = 3.23 \mu\text{G}$ ,  $c_s = 5 \text{ km s}^{-1}$ , and  $z_d = 200 \text{ pc}$ . Since these values are typical in the solar neighbourhood, this model can be regarded as a standard one. In the equilibrium the magnetic field runs in the  $x$ -direction and the perturbation is set to be proportional to  $\sin(kx)$ . The thin and thick curves denote the growth rate ( $\omega_i$ ) as a function of the wave number ( $k$ ) for even and odd modes, respectively. The even mode fragments the galactic disk, maintaining its symmetry with respect to the galactic plane, while the perturbation is anti-symmetric in the odd mode. The even mode is mainly driven by the Jeans instability while the odd mode is mainly driven by the Parker instability. In this standard model the growth of the odd mode is dominant (cf. Horiuchi *et al.* 1988; Giz & Shu 1993). The odd mode has the maximum,  $1.52 \times 10^{-8} \text{ yr}^{-1}$ , when the wavelength is  $2\pi/k = \lambda = 800 \text{ pc}$ .

Figure 3 shows the dispersion relation for a gas-rich disk (model 3 of HNN). The model parameters are set  $n_c = 4 \text{ cm}^{-3}$ ,  $B_c = 6.46 \mu\text{G}$ ,  $v_\varphi = 220 \text{ km s}^{-1}$ ,  $c_s = 5 \text{ km s}^{-1}$ , and  $z_d = 200 \text{ pc}$ . The even mode is dominant over the even mode in this model. The growth rate is maximum ( $\omega_i = 2.80 \times 10^{-8} \text{ yr}^{-1}$ ) at  $\lambda = 890 \text{ pc}$ . We presume that our galactic disk was gas-rich in the early stage. The stability of the early galactic disk was presumably very different from that of the present one.

The dispersion relation depends also on the other parameters. When  $z_d$  is larger, the growth rate is also larger, mainly because the Parker instability is enhanced by a higher  $g_z$ . When magnetic fields are weaker (smaller  $B_c$ ), both the odd mode and the

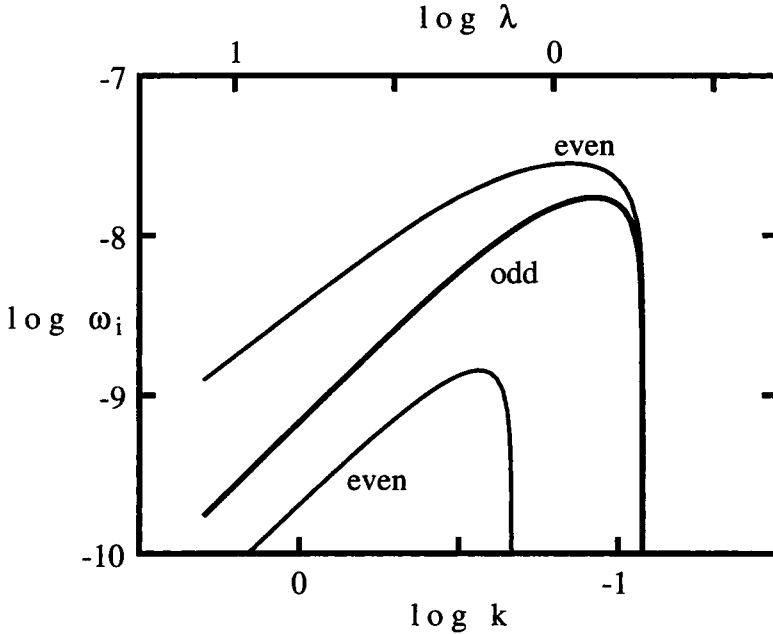


FIGURE 3. The same as Figure 2 but for  $n_c = 4 \text{ cm}^{-3}$  and  $B_c = 6.46 \text{ } \mu\text{G}$ . Reproduced from Figure 1b of HNN.

even mode have a lower growth rate. This is because the stabilising effect of rotation is cancelled by angular-momentum transfer through magnetic torque (Lynden-Bell 1966). These dependences are summarised in an approximate dispersion relation

$$\omega^2 = \frac{\nu_m^2(\nu_s^2 - \nu_P^2)}{(\nu_s^2 + \nu_P^2)(1 + \nu_m^2/\nu_s^2)}, \tag{3.6}$$

for the odd mode where the Parker frequency  $\nu_P$  is defined as

$$\nu_P = \frac{g}{2c_s} (1 + \nu_m^2/2\nu_s^2)^{-1/2} \tag{3.7}$$

$$= 2.97 \times 10^{-15} \left( \frac{g_z}{4.2 \times 10^{-9} \text{ cm s}^{-1}} \right) \left( \frac{c_s}{5 \text{ km s}^{-1}} \right) (1 + \nu_m^2/2\nu_s^2)^{-1/2} \text{ Hz}. \tag{3.8}$$

Similarly the even mode has an analytic approximate dispersion relation (see HNN).

#### 4. Non-linear evolution

In this section we show the non-linear evolution of the instabilities for both odd and even modes. The non-linear evolution was followed with two-dimensional numerical simulations. By assuming the glide reflection symmetry for the odd mode and the mirror symmetry for the even mode, the computation domain is reduced to  $0 \leq x \leq \lambda/2$  and  $0 \leq z \leq z_d$ . The corresponding boundary conditions are set at  $x = 0$  &  $\lambda/2$  and  $z = 0$ . Out of the boundary of  $z = z_d$  buffer layers are set to mimic a hot dilute gas there. In the buffer layers the gravity is set to vanish. The spatial resolution is  $\Delta x = \Delta z = 2 \text{ pc}$  in the simulations. The magnetohydrodynamical equations are integrated with an upwind scheme (see Hanawa *et al.* 1994) for the difference scheme. It is a virtue of an upwind scheme that the obtained numerical solutions are free from artificial oscillations.

In the numerical simulations, horizontal velocity perturbation is imposed on an equi-

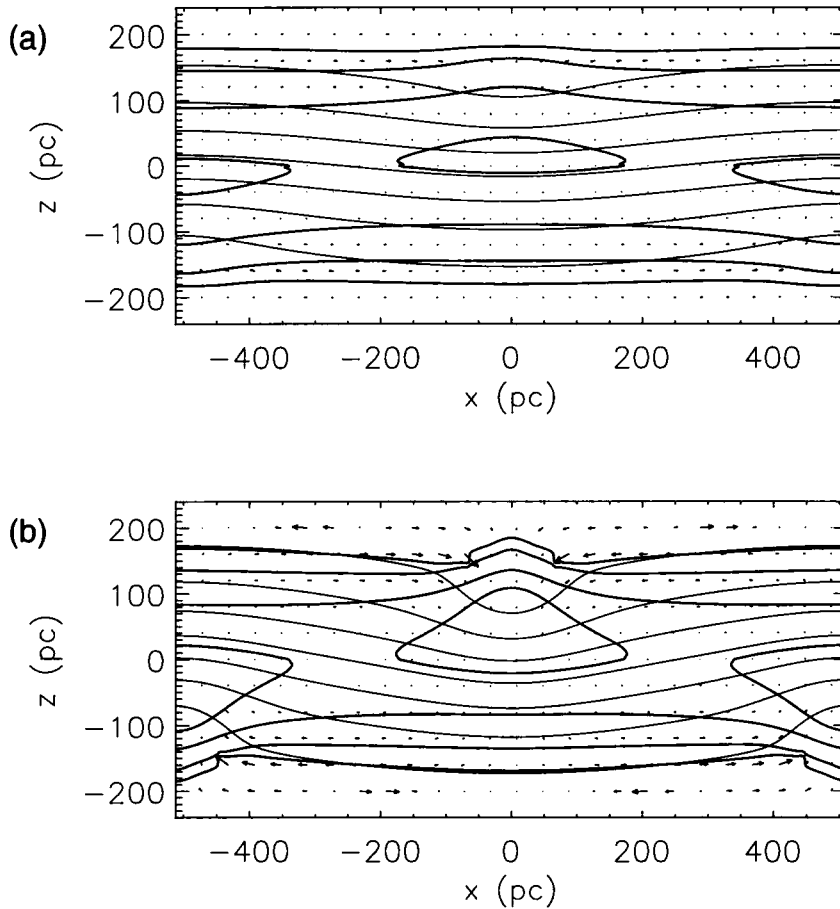


FIGURE 4. The evolution of the perturbation with the glide reflection symmetry. The upper and lower panels show the stages at which the time passed  $9.2 \times 10^7$  and  $1.4 \times 10^8$  y, respectively. The thick curves denote the density contours of  $n = 0.1, 0.2, 0.5,$  and  $1.0 \text{ cm}^{-3}$ . The thin curves denote the magnetic lines of force. The mass and magnetic field densities are  $n = 1 \text{ cm}^{-3}$  and  $B = 3.23 \text{ } \mu\text{G}$ , respectively, on the galactic plane at the initial model.

librium model. Figure 4 shows the evolution of a velocity perturbation with the glide reflection symmetry. Initially, the density has its maximum ( $n = 1 \text{ cm}^{-3}$ ) on the galactic plane. The sound speed is set as uniform and constant ( $c_s = 5 \text{ km s}^{-1}$ ). The rotation is not taken into account in this model. The thick curves are the contours of equal densities of  $n = 0.1, 0.2, 0.5,$  and  $1.0 \text{ cm}^{-3}$  while the thin curves denote lines of magnetic force. Figures 4a and b show the stages at which the time passed  $9.2 \times 10^7$  yr and  $1.4 \times 10^8$  y, respectively, from the initial. The maximum density is  $1.05$  and  $1.52 \text{ cm}^{-3}$  in figures 4a and b, respectively. The instability forms density enhancements off the galactic plane. They are located in the magnetic valleys and supported in part by the magnetic fields. Gas slides down to the valley along the field line. The density enhancements are bounded by shock waves in the regions of high  $|z|$  (Matsumoto *et al.* 1988).

Figure 5 shows the evolution of a velocity perturbation with the mirror symmetry. The initial density and magnetic field distributions are the same as those for the glide

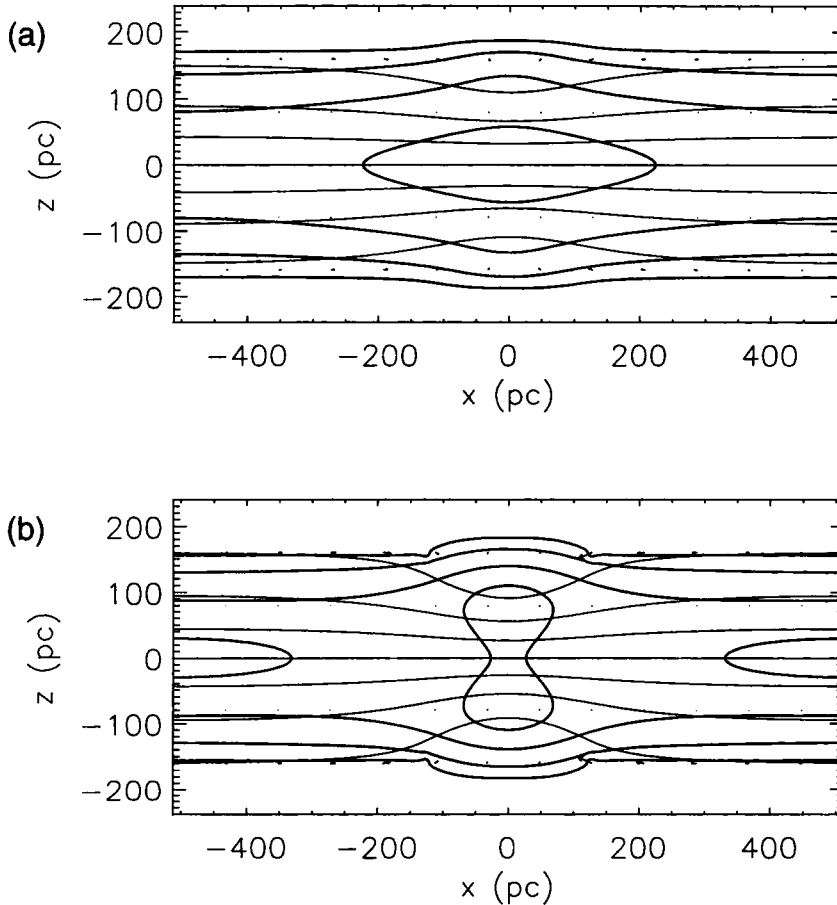


FIGURE 5. The evolution of the perturbation with the mirror symmetry. The upper and lower panels show the stages at which the time passed  $1.13 \times 10^8$  and  $1.67 \times 10^8$  y, respectively, from the initial model. The thick curves denote the density contours of  $n = 0.1, 0.2, 0.5,$  and  $1.0 \text{ cm}^{-3}$ . The thin curves denote the magnetic lines of force. The mass and magnetic field densities are  $n = 1 \text{ cm}^{-3}$  and  $B = 3.23 \text{ } \mu\text{G}$ , respectively, on the galactic plane at the initial model.

reflection symmetry. Figures 5a and b show the stages at which the time passed  $1.13 \times 10^8$  and  $1.67 \times 10^8$  y, respectively. The density has its maximum at  $(x, z) = (0, 0)$  in early stages while it has the maximum at  $(x, z) = (512 \text{ pc}, 0)$  in late stages. The second density enhancement is formed by the reverse flow from the first one, which is not gravitationally bound. The second density enhancement may also be dissolved to form the third density enhancement. (See Matsumoto *et al.* 1990 for the nonlinear oscillation of the Parker instability).

Figure 6 shows the evolution of a velocity perturbation with the mirror symmetry in a gas-rich disk. At the initial state the mirror symmetric velocity perturbation was superimposed on an equilibrium model of  $n_c = 4 \text{ cm}^{-3}$ ,  $B_c = 6.46 \text{ } \mu\text{G}$ ,  $v_\varphi = 0$ ,  $c_s = 5 \text{ km s}^{-1}$ , and  $z_d = 200 \text{ pc}$ . Figures 6a and b show the stages at which the time passed  $4.94 \times 10^7$  and  $6.88 \times 10^7$  yr, respectively. The maximum density is  $6.52$  and  $12.23 \text{ cm}^{-3}$  in figures 6a and b, respectively. In this model the maximum density in-

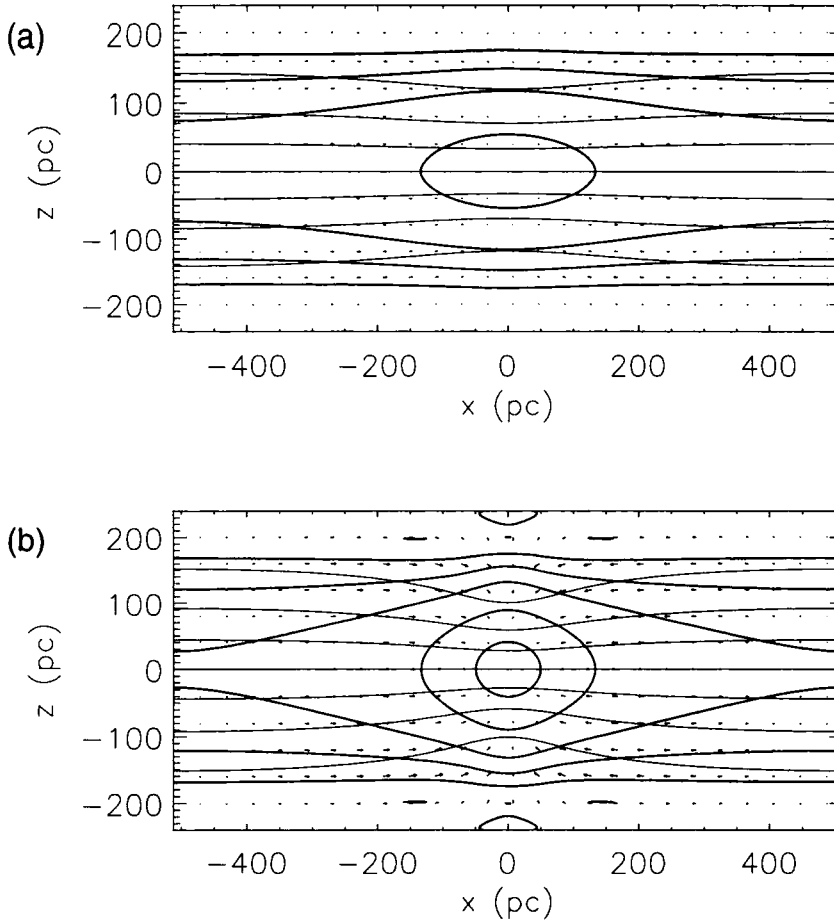


FIGURE 6. The evolution of the perturbation with the mirror symmetry in a gas-rich disk. The upper and lower panels show the stages at which the time passed  $1.13 \times 10^8$  and  $1.67 \times 10^8$  y, respectively, from the initial model. The thick curves denote the density contours of  $n = 0.5, 1.0, 2.0, 5.0,$  and  $10.0 \text{ cm}^{-3}$ . The thin curves denote the magnetic lines of force. The mass and magnetic field densities are  $n = 4 \text{ cm}^{-3}$  and  $B = 6.46 \mu\text{G}$ , respectively, on the galactic plane at the initial model.

creases monotonically and unboundedly. The density enhancement formed by instability collapses unboundedly when its line density exceeds a critical value,

$$\begin{aligned} \ell_{\text{cr}} &= 2c_s^2/G \\ &= 7.5 \times 10^{18} \left( \frac{c_s}{5 \text{ km s}^{-1}} \right)^2 \text{ g cm}^{-1}. \end{aligned} \tag{4.9}$$

Otherwise the density enhancement remains gravitationally unbound. The even-mode instability produces the density enhancement having the line density,

$$\ell = 3.15 \times 10^{18} \left( \frac{n}{1 \text{ cm}^{-3}} \right) \left( \frac{\lambda}{1 \text{ kpc}} \right) \left( \frac{H}{100 \text{ pc}} \right) \text{ g cm}^{-1}, \tag{4.10}$$

where  $\lambda$  and  $H$  are the wavelength of the perturbation and the half thickness of the gas disk. Note that  $\ell$  is close to  $\ell_{\text{cr}}$ .

## 5. Summary

As shown above, the instability of the galactic gaseous disk is influenced by many factors, i.e. gravity of stars and gas clouds, magnetic fields, rotation, thermal pressure, and turbulence. It is shown that the stability of the galactic disk depends sensitively on the model parameters. This is because gravity, rotation and magnetic fields have coupled effects and the result is the delicate balance between the competing processes. In this sense, minor effects may also have significant influences on the instability. Although our model takes account of many factors, it is still simple and lacks other factors such as differential rotation and spiral arms (cf. Foglizzo & Tagger 1994; Foglizzo, this volume). Incorporating these effects is a problem for the future.

The author would like to acknowledge the collaborations of Drs. Fumitaka Nakamura and Yasushi Nakajima and thank them for their permission to include their unpublished simulations in this paper.

## REFERENCES

- FOGLIZZO, T. & TAGGER, M. 1994 *Astron. Astrophys.* **287**, 297.  
 GIZ, A. T. & SHU, F. H. 1993 *Astrophys. J.* **404**, 185.  
 HANAWA, T., NAKAJIMA, Y. & NOBUTA, K. 1994 *J. Comp. Phys.* submitted (DPNU-94-34).  
 HANAWA, T., NAKAMURA, F. & NAKANO, T. 1992 *Publ. Astron. Soc. Jpn.* **44**, 509.  
 HORIUCHI, T., MATSUMOTO, R., HANAWA, T. & SHIBATA, K. 1988 *Publ. Astron. Soc. Jpn.* **40**, 147.  
 LYNDEN-BELL, D. 1966 *Observatory* **86**, 57.  
 MATSUMOTO, R., HORIUCHI, T., HANAWA, T. & SHIBATA, K. 1990 *Astrophys. J.* **356**, 259.  
 MATSUMOTO, R., HORIUCHI, T., SHIBATA, K. & HANAWA, T. 1988 *Publ. Astron. Soc. Jpn.* **40**, 171.

**Elmegreen:** When does the even mode dominate?

**Hanawa:** The even mode dominates when the mass of the gas disk is more than half the total mass of the disk including disk stars.

**Lesch:** What is the role of turbulent diffusion in your model?

**Hanawa:** At the present stage, we restrict ourselves to the dynamical processes of short timescales and our model does not take account of turbulent diffusion.

**Shore:** First a comment. Your first viewgraph shows wonderfully that all of the growth times are wonderfully close—a little miracle of self-regulation. Maybe this is only because gravity is the source of everything. Now, to questions. First, where are the shocks in your model? And the second, you have large shear in some regions so the Kelvin–Helmholtz instability should lead to a turbulent cascade. Why is turbulence not included in the models? It will change the critical line density,  $\ell_{\text{crit}}$ , as a function of density. It should be easy to include this in your model since you have a map of the velocity field.

**Hanawa:** Shocks are formed at the interfaces between the down flows and the density enhancements. The shocks are stronger in the regions of higher  $z$ . Figures 4b and 5b show the density and velocity discontinuities at the shock fronts. Now, to the second question. If the turbulent velocity increases, the critical line density increases. I do not, however, agree with your opinion that velocity shear induces the Kelvin–Helmholtz instability in our model simulations.



# Galactic Disk Dynamics and Magnetic Field Evolution

By HARALD LESCH

Max-Planck-Institut für Radioastronomie, Auf dem Hügel 69, D-53121 Bonn, Germany

The Milky Way and the nearby disk galaxies contain large-scale magnetic fields. This is clearly shown by the high-frequency radio polarisation measurements, which also show that the large-scale magnetic field structure is connected to the overall velocity field of the interstellar gas. The magnetic field in the conductive plasma of the interstellar medium is subject to turbulent diffusion, i.e. it has to be amplified and sustained against diffusive losses via gas motions. The galactic dynamo describes the interplay of amplification via differential shear and turbulence on one side and turbulent diffusion on the other side. Such an axisymmetric dynamo takes a few gigayears to amplify the magnetic field. In the light of observations at high redshifts ( $z = 2$ ) which already indicate a  $\mu$ Gauss field the axisymmetric dynamos are too slow. Thus, we consider the influence of large-scale non-axisymmetric gravitational instabilities (bars, spirals, oval distortions, etc.) on the gas motion and the coupled magnetic field. The timescale for the field amplification due to non-axisymmetric velocity fields is related to the timescale of angular momentum transport. Due to its dissipation properties, the gas plays the major role for the excitation of non-axisymmetric features. Since the magnetic field amplification also takes place in the interstellar gas we consider the interplay of gas dynamical processes triggered by gravitational instabilities and magnetic fields. A comparison of the timescales shows that field amplification by non-axisymmetric velocity fields is faster than an axisymmetric dynamo.

---

## 1. Introduction

The Milky Way is a magnetised disk. It contains a large-scale magnetic field, which exhibits several reversals, as indicated by Faraday-rotation measures of pulsars and extragalactic objects. Although there is no general consensus about such field reversals, evidence is now accumulating that within the central 5 kpc the magnetic field indeed changes its direction several times, indicating a so-called bisymmetric field structure (Rand & Lyne 1994). The regular field resembles the spiral structure and is mainly confined in the galactic plane. The strength of the large-scale component is about 3  $\mu$ Gauss (Wielebinski 1993; Han & Qiao 1993). Radio surveys of the galactic plane offer even more details about the magnetic field structure. However, we cannot delineate much of the information because of our “insider” view of the Galaxy. Thus, radio observations of other galaxies obviously help to understand our own magnetised galaxy.

The magnetic field structure in other galaxies is most easily visible at high frequencies, where the Faraday rotation is negligible. At  $\lambda$  2.8 cm, the Faraday rotation is less than 5 degrees. Therefore, a polarisation measurement at this wavelength gives a direct picture of the magnetic field configuration. (For a review about the status of high-frequency polarisation measurements, see Beck 1993.) I will briefly summarise the main results of the observations. The lines of force are well aligned with characteristic features of a disk galaxy such as spiral and bars, and in only a few of all edge-on galaxies prevail large-scale vertical fields perpendicular to a disk. Attempts to derive actual directions of magnetic vectors are rather delicate tasks with a lot of ambiguities, and are not decisive in revealing whether or not field directions change along the azimuth in a galactic disk. However, at least three examples have been found which show some evidence for a well-defined field structure: M31 and IC342 exhibit an axisymmetric field, and M81

contains a bisymmetric field structure (M. Krause 1990). High-frequency measurements (Neininger *et al.* 1991; Neininger 1992) suggest that the magnetic morphology is principally associated with non-axisymmetric galactic structures, such as bars or spiral arms, accompanying a large-scale gas flow.

It has been argued that the present magnetic field structure and typical strength of galactic magnetic fields are organised by induction processes called  $\alpha - \Omega$ -dynamo (Parker 1971; Vainshtein & Ruzmaikin 1972). We critically review this model in the next section. The problems of this axisymmetric description will lead us to investigate non-axisymmetric amplification mechanisms, which may not only explain the present status of galactic magnetic fields, but also describe the evolution of magnetic fields in high-redshift objects, which seem to contain magnetic field strengths already  $\sim \mu\text{Gauss}$ , comparable with the present field strengths in nearby spirals (Kronberg 1994).

## 2. Galactic plasmaphysics I

The spatial and time evolution of magnetic fields is described by the *induction equation*, which can be derived from the Maxwell's equation and Ohm's law:

$$\frac{\partial \mathbf{B}}{\partial t} = \nabla \times (\mathbf{v} \times \mathbf{B} - \eta(\nabla \times \mathbf{B})), \quad (2.1)$$

where  $\eta = \frac{c^2}{4\pi\sigma}$  is the magnetic diffusivity, with the electrical conductivity  $\sigma$ . If  $\sigma$  is determined by Coulomb collisions the magnetic field is strongly coupled to plasma flow with velocity  $\mathbf{v}$  (often stated as “frozen-in”-field), since  $\sigma \propto T^{3/2}$  is very large, which means  $\eta$  is very small and the characteristic diffusion timescale  $t_d \propto \frac{L^2}{\eta}$  is very large. For galactic length scales (few kiloparsecs) the diffusion timescale due to classical diffusivity is of the order  $10^{27}$  yr !

There is no source term in Equation (2.1), i.e. there is no outright creation of magnetic field in the hydromagnetic description. The contemporary magnetic fields can be sustained against resistive decay only by amplification of the existing magnetic field flux, rather than by the fresh creation of magnetic fields. Hence, if at any point in time the Universe was devoid of magnetic fields, then as far as hydromagnetic effects are concerned, there would be no magnetic field at any other time.

Biermann (1950) made the point that there are microscopic thermal and inertial “battery” effects in a moving ionised gas. These battery effects are overlooked by the hydromagnetic approximation of the gas as a classical resistive fluid. The importance of battery effects is that they guarantee that, if all else fails, the stars and galaxies are seeded with magnetic fields. The typical seed field values are of the order of  $10^{-18}$  G (Lesch & Chiba 1995).

Equation (2.1) gives a qualitative description about the mechanisms involved: the velocity field of the plasma increases the field strength, whereas the resistance reduces the field strength. Only little is known about the resistance of the galactic plasma. Observationally we have much more information about the motions in the interstellar medium (ISM) of the Milky Way. The gas in the disk rotates differentially, with velocities of about  $200 \text{ km s}^{-1}$  and exhibits a velocity dispersion of more than  $10 \text{ km s}^{-1}$  at the solar neighbourhood, increasing towards the centre (Stark *et al.* 1991).

Nevertheless, the controversial discussion about the origin and fate of galactic magnetic fields concentrates on the question of what kind of diffusivity is acting in galaxies. If the diffusivity is very small ( $\leq 10^{23} \text{ cm}^2 \text{ s}^{-1}$ ), the existence of primordial magnetic fields is enough to explain the contemporary magnetic fields, since they do not simply decay